Molecular Biology of the Cell
Vol. 17, 2138–2149, May 2006

Function of the Neuron-specific Alternatively Spliced Isoforms of Nonmuscle Myosin II-B during Mouse Brain Development

Xuefei Ma, Sachiyo Kawamoto, Jorge Uribe, and Robert S. Adelstein

Laboratory of Molecular Cardiology, National Heart, Lung, and Blood Institute, National Institutes of Health, Bethesda, MD 20892

Submitted October 31, 2005; Revised January 17, 2006; Accepted February 6, 2006
Monitoring Editor: Erika Holzbaur

We report that the alternatively spliced isoforms of nonmuscle myosin heavy chain II-B (NHMC II-B) play distinct roles during mouse brain development. The B1-inserted isoform of NMHC II-B, which contains an insert of 10 amino acids near the ATP-binding region (loop 1) of the myosin heavy chain, is involved in normal migration of facial neurons. In contrast, the B2-inserted isoform, which contains an insert of 21 amino acids near the actin-binding region (loop 2), is important for postnatal development of cerebellar Purkinje cells. Deletion of the B1 alternative exon, together with reduced expression of myosin II-B, results in abnormal migration and consequent protrusion of facial neurons into the fourth ventricle. This protrusion is associated with the development of hydrocephalus. Restoring the amount of myosin II-B expression to wild-type levels prevents these defects, showing the importance of total myosin activity in facial neuron migration. In contrast, deletion of the B2 alternative exon results in abnormal development of cerebellar Purkinje cells. Cells lacking the B2-inserted isoform show reduced numbers of dendritic spines and branches. Some of the B2-ablated Purkinje cells are misplaced in the cerebellar molecular layer. All of the B2-ablated mice demonstrated impaired motor coordination.

INTRODUCTION

Humans and mice express three different genes that encode nonmuscle myosin heavy chain II (NMHC) isoforms. The genes in humans are referred to as *MYH9*, *MYH10*, and *MYH14*, and their protein products are commonly called NMHC II-A, II-B, and II-C, respectively. A pair of myosin heavy chains along with two pairs of light chains constitute the nonmuscle myosin II molecule, and each of these proteins seems to play a role in cell motility (Svitkina *et al*., 1997; Ma *et al*., 2004), cell morphology (Wei and Adelstein, 2000), cell adhesion (Conti *et al*., 2004), and cytokinesis (De Lozanne and Spudich, 1987; Takeda *et al*., 2003; Bao *et al*., 2005).

Evidence from a number of laboratories has shown that nonmuscle myosin II-A and II-B have different functions in the same cell (Chantler and Wylie, 2003; Kolega, 2003; Lo *et al*., 2004; Meshel *et al*., 2005), and work from this laboratory has demonstrated a different role for nonmuscle myosin II-A and II-B during mouse development. Whereas ablation of NMHC II-A results in defects in cell adhesion and visceral endoderm maturation, and is lethal by embryonic day (E) 7.5 (Conti *et al*., 2004), ablation or mutation of NMHC II-B results in specific defects in the heart and brain and is lethal by E13.5–16.5 (Takeda *et al*., 2003; Ma *et al*., 2004).

This article was published online ahead of print in *MBC in Press* (http://www.molbiolcell.org/cgi/doi/10.1091/mbc.E05–10–0997) on February 15, 2006.

Address correspondence to: Robert S. Adelstein (adelster@nhlbi.nih.gov).

Abbreviations used: E, embryonic day; ES, embryonic stem; HMM, heavy meromyosin; Neo^r, neomycin resistance; NMHC, nonmuscle myosin heavy chain; P, postnatal day; PBS, phosphate-buffered saline.

Two of the three NMHCs, II-B and II-C, have been shown to undergo alternative splicing of pre-mRNAs in which an exon encoding either 10 (II-B) or 8 (II-C) amino acids is inserted into the loop near the ATP-binding region of the NMHC (Takahashi *et al*., 1992; Golomb *et al*., 2004). This is the same location into which an alternative exon encoding seven amino acids is inserted in the smooth muscle MHC where the insert seems to play a role in determining whether the muscle is phasic or tonic (Kelley *et al*., 1993; Karagiannis *et al*., 2003). In all three cases, baculovirus-expressed heavy meromyosins (HMMs) containing the alternative exon show increased actin-activated MgATPase activity and in vitro motility in translocating actin filaments, compared with HMMs without the alternative exon (Kelley *et al*., 1993; Pato *et al*., 1996; Kim *et al*., 2005). A second alternative exon encoding 21 amino acids is inserted into loop 2 in the actin-binding region of NMHC II-B (Takahashi *et al*., 1992). We refer to the first of these inserted isoforms of NMHC II-B as the B1-inserted isoform and the second of these as the B2-inserted isoform. A recent search of the human and mouse genome sequences reveals the presence of an alternative exon in loop 2 of NMHC II-C (our unpublished data). Previous work has demonstrated that both the B1- and B2-inserted isoforms of NMHC II-B were expressed in the neuronal cells of avians and mammals and that they differed in the time at which they were first expressed (Itoh and Adelstein, 1995). Whereas the B1-inserted isoform was expressed during embryonic development, the B2-inserted isoform was only expressed after birth.

Alternative splicing of pre-mRNA is an important mechanism for regulating gene expression in higher eukaryotic organisms (Guo and Kawamoto, 2000; for review, see Stamm *et al*., 2005). More than half of human genes use alternative splicing to increase proteome diversity. How-

ever, the in vivo significance of most alternatively spliced isoforms has not been verified, and only a few reports to date have dealt with the in vivo function of these isoforms (Babu *et al*., 2001; Xu *et al*., 2005). The goal of the present study was to elucidate the function of the two alternatively spliced isoforms of NMHC II-B during mouse brain development.

Our laboratory previously generated mice in which the exon encoding the B1 insert was replaced with the cassette conferring neomycin resistance (Neo^r; Uren *et al*., 2000). Some of the homozygous B1 insert-ablated mice developed an overt, progressive hydrocephalus and mislocalization of a group of neurons. Although useful for studying the effects of gene dosage, results from these mice were somewhat confounded because of a general decrease in the expression of total NMHC II-B, which is often seen when the Neo^r cassette is introduced into an intron or is used to replace an alternative exon (Fiering *et al*., 1995; Meyers *et al*., 1998). With respect to the B2-inserted isoform, previous work has shown that both the temporal and regional expression pattern of this isoform in rats suggested a role in the regulation of cerebellar development (Miyazaki *et al*., 2000). It was predominantly expressed in rat cerebellum, especially in cerebellar Purkinje cells. However, no in vivo studies have been performed on the specific function of this isoform to date. We hypothesized that the B1- and B2-inserted isoforms of NMHC II-B play distinct roles during brain development. To test this hypothesis, we generated insert-ablated mice.

Here, we report on the results of ablating either the exon encoding the B1 insert or the exon encoding the B2 insert of NMHC II-B in mice using homologous recombination. We show that ablation of each of these alternative exons results in a distinct phenotype and that, in the case of ablation of the B1 insert, the phenotype is influenced by the amount of myosin II-B. These studies demonstrate that ablation of B1-inserted myosin results in the abnormal migration of facial neurons, which is associated with the development of hydrocephalus. In contrast, ablation of B2-inserted myosin results in abnormal maturation of cerebellar Purkinje cells, regardless of the expression level of noninserted NMHC II-B. As a consequence of these cerebellar defects, the B2-insert–ablated mice have difficulties in maintaining their balance compared with wild-type and heterozygous littermates.

MATERIALS AND METHODS

Reverse Transcription-PCR Analysis of the Inserted NMHC II-B

Expression of the inserted isoforms of NMHC II-B was analyzed by reverse transcription (RT)-PCR in adult mice using primers as indicated in Figure 1A. PCR products were separated using agarose gel electrophoresis. To estimate the relative amount of the B1- or B2-inserted isoforms compared with the B1- or B2-noninserted isoforms, primer sets flanking either the alternative exon B1 (primers P1 and P2) or B2 (P3 and P4) were used. The inserted isoform contained an extra 30 (B1) or 63 (B2) nucleotides compared with the noninserted isoform. Because NMHC II-B could contain both the B1 and B2 insert, we next carried out RT-PCR analyses by first amplifying only the isoforms that contained the B1 insert, including the B1 single-inserted as well as the B1 and B2 double-inserted isoforms using primers P5 and P4. After nested PCR using primers P3 and P4, the B1 and B2 double-inserted isoform was separated from the B1 single-inserted isoform because it contained an extra 63 nucleotides. Similarly, by first amplifying only the B2-inserted isoforms using primers P1 and P6, followed by a nested PCR using primers P1 and P2, the doubly inserted isoform was separated from the B2 single-inserted isoform because it contained an extra 30 nucleotides. To assess the relative abundance of the noninserted isoform of NMHC II-B (which contains neither the B1 nor the B2 insert), we first amplified the B1 insert-excluded isoforms that contained the B2-inserted and noninserted isoforms using primer P7 and P4 and then carried out a nested PCR using the primers P3 and P4 to separate the B2 single-inserted isoform from noninserted isoform. Similarly, using primers P1 and P8, followed by a nested PCR using primers P1 and P2, the B1 single-inserted isoform was separated from the noninserted isoform. Table 1 summarizes the quantification of these isoforms for various parts of the brain and spinal cord. The expression of inserted isoforms of NMHC II-B was also evaluated for embryonic mouse brains. Insert-specific primers were used to detect whether either of the alternative exons was expressed. The primers used for the B1 insert were P5 and P2 and for the B2 insert were P3 and P6. Postnatal temporal expression of B2-inserted isoforms was performed using primers P3 and P4. The PCR products were radioactively labeled using [α-^{32}P]dCTP and separated on a 6% polyacrylamide urea-Tris borate-EDTA gel.

Gene Targeting and Generation of Insert-ablated Mice

Genomic fragments containing alternative exon B1 or B2 and surrounding regions of the NMHC II-B gene obtained from a 129/Sv mouse genomic library (Stratagene, La Jolla, CA) were selected for targeting vector construction (Figure 2, A and B). The alternative exons, including part of their surrounding intronic sequences, were replaced by floxed Neo^r cassettes. The diphtheria toxin-A cassette was inserted at the 3′ end of the constructs for

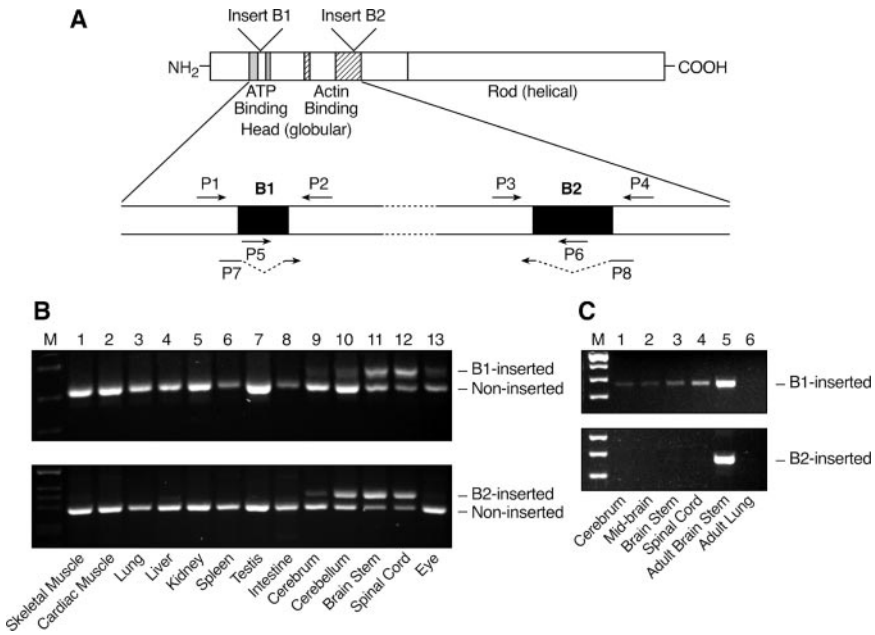

Figure 1. Expression of alternatively spliced isoforms of NMHC II-B in mice. (A) Diagram of NMHC II-B transcripts shows location of the alternative exons and primers used in RT-PCR analysis. (B) RT-PCR analysis of the B1- and B2-inserted NHMC II-B from tissues of adult mice using primers P1 and P2 for B1 insert (top) and P3 and P4 for the B2 insert (bottom). The B1 and B2 insert are only present in neuronal tissues. (C) RT-PCR analysis of the expression of the B1 and B2-inserted NMHC II-B in embryonic mouse brain (E12.5) using primers P5 and P2 for B1 insert (top) and P3 and P6 for B2 insert (bottom). Only the B1 insert is detected in embryonic brain and spinal cord. Adult mouse brain stem is included as a positive control, and adult mouse lung is used as a negative control.

Table 1. Distribution of nonmuscle myosin heavy chain II-B isoforms in adult mouse brain

	Cerebrum	Cerebellum	Brain stem	Spinal cord
B1 single inserted	5	5	10	15
B2 single inserted	10	40	25	15
B1 + B2 double inserted	5	5	50	50
Noninserted	80	50	15	20

Values are expressed as percentages.

negative selection. The linearized plasmids were electroporated into CMT-1 embryonic stem (ES) cells (Specialty Media, Division of Cell and Molecular Technologies, Phillipsburg, NJ) and selected with Geneticin (G418). Genomic DNA isolated from G418-resistant ES cell clones was analyzed using Southern blotting with the 3′ external probes indicated in Figure 2, A and B, to identify targeted ES cell clones. To generate chimeric mice, targeted ES cells were injected into blastocysts derived from C57BL/6 mice. Mice were maintained in a 129/SvXC57BL/6 background for phenotype analysis. Genotyping of progeny was carried out by Southern blot or PCR using genomic DNA isolated from mouse tails. To remove the floxed Neo^r cassette, the homozygous mice were crossed with mice expressing Cre-recombinase under control of the cytomegalovirus promoter (Balb/C CMV-Cre; The Jackson Laboratory, Bar Harbor, ME). All procedures were conducted following an approved animal protocol in accordance with the National Heart, Lung, and Blood Institute Animal Care and Use Committee.

Preparation and Characterization of Antibodies Specific for the B2-inserted NMHC II-B

Affinity-purified rabbit polyclonal antibodies against the entire 21 amino acid sequence of the mouse B2 insert were generated. The sequence used was: -EIQTIQRASFYDSVSGLHEPP-. The antibodies were characterized by immunoblotting (1:1000 dilution) using protein extracts from an adult mouse cerebellum as a positive control and extracts from a wild-type mouse lung (where no mRNA encoding the B2-inserted NMHC II-B was detected) and B2-ablated mouse cerebellum as negative controls (Figure 7). Immunoblot analyses were carried out as described previously (Phillips *et al*., 1995; Takeda *et al*., 2000). Generation of B1-inserted NMHC II-B–specific antibodies was also attempted. Despite multiple attempts, we were unable to obtain antibodies.

Histology and Immunostaining

The mouse embryos were collected in phosphate-buffered saline (PBS) and immediately immersed into 4% paraformaldehyde in PBS, pH 7.4, after the brain was exposed by partially removing the skin and skull. For fixation of adult mouse brains, mice were slowly perfused with fixative through the cardiac left ventricle after making an incision into the right atrium. The brains were then dissected out from the skull and immersed in the same fixative overnight at 4°C. Five-micrometer-thick paraffin sections were prepared. For histological analysis, the sections were stained with H&E. For immunofluorescence staining, samples were blocked with PBS containing 0.1% bovine serum albumin/5% normal goat serum for 1 h at room temperature. They were then incubated with polyclonal antibodies against NMHC II-B (1:3000; Phillips *et al*., 1995), B2-inserted NMHC II-B (1:100), glial fibrillary acidic protein (1:500; DakoCytomation, Glostrup, Denmark), or calbindin (1:10,000; Sigma-Aldrich, St., Louis, MO) overnight at 4°C; followed by incubation with fluorescein isothiocyanate or Texas Red-conjugated goat anti-rabbit or goat anti-mouse IgG (1:200; Jackson ImmunoResearch Laboratories, West Grove, PA) for 1 h at room temperature and counterstained with 4,6-diamidino-2-phenylindole (DAPI). F-actin was visualized by rhodamine phalloidin (1:500;

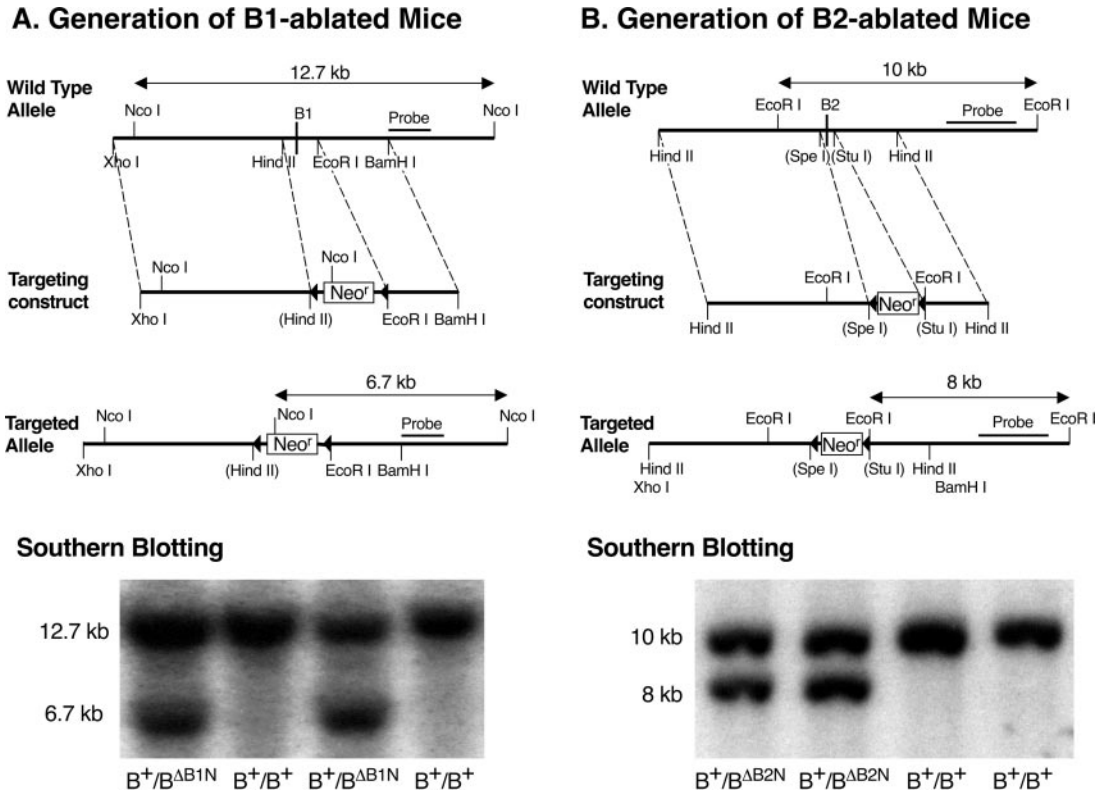

Figure 2. Generation of NMHC II-B alternative exon B1- or B2-ablated mice. (A) Ablation of exon B1. Diagrams of the wild-type allele, targeting construct and targeted allele for the generation of exon B1-ablated mice are shown. The HindII/EcoRI fragment containing the alternative B1 exon was replaced by a floxed Neo^r cassette. Bottom, Southern blot used for screening ES cell clones. Genomic DNA isolated from ES cell clones was digested with NcoI and probed with the indicated fragment. The wild-type allele generated a 12.7-kb fragment, whereas the targeted allele generated a 6.7-kb band. (B) Ablation of exon B2. The SpeI/StuI fragment containing the alternative B2 exon was replaced by a floxed Neo^r cassette. Bottom, Southern blot used for screening ES cell clones. Genomic DNA was digested by EcoRI and probed with the indicated fragment. The wild-type allele generated a 10-kb band, and the targeted allele generated an 8-kb band. Note that the constitutive exons are not shown.

Molecular Probes, Eugene, OR). Rabbit or mouse IgG was applied in place of the primary antibody as a negative control. After washing, the coverslips were mounted using a ProLong Antifade kit (Molecular Probes). The images were collected using an SP confocal microscope (Leica, Deerfield, IL). For immunohistochemistry, after incubation with the primary antibody specific for B2-inserted NMHC II-B, a Vectastain ABC Elite kit (Vector Laboratories, Burlingame, CA) was used for signal detection.

Quantification of Migrating Facial Neurons

A major phenotype observed in the hypomorphic B1 insert-deleted mice was the abnormal migration of facial neurons resulting in their protrusion into the fourth ventricle. All of the B1 insert-ablated mice analyzed (>10) showed this abnormality, and none of the wild-type or heterozygous mice showed the abnormality. Quantification of the exact number of the protruding facial neurons in the mutant mice was difficult because the protruding mass contains other cells such as glial cells. In contrast, some of the facial neurons in the B1 insert–ablated mice did migrate to their normal location, and we were able to count them based on their distinct morphology and localization and to compare the number of these cells to the number of cells reaching their normal location in wild-type mouse brains. We did this on two separate days during embryonic development (E14.5 and E16.5) after the facial neurons had completed their migration. We prepared serial 5-μm sagittal sections of mouse brains and found that ~100 sections contained all the facial neurons. We therefore counted the facial neurons in one of 10 sections for each mouse after H&E staining of sections. In total, we counted facial neurons from eight embryonic mouse brains (4 wild types and 4 hypomorphic B1-insert–ablated mice).

Motor Coordination Analysis

Motor coordination activity was evaluated in adult mice (4 mo old) using a rotarod (UGO Basile, Siena, Italy). Five mice were tested at a time in individual compartments. Rotation of the rod was not started until all mice were successfully balanced on the stationary rod. Mice that fell before the start were repositioned, and the fall was not counted. The rod was then rotated at three different rates of 20, 32, and 40 rpm, and the latency to fall was measured by separate electronic timers for each mouse. The maximum time for each trial was set for 60 s. Mice that exceeded 60 s were stopped and scored as 60 s for their latency. All trials were observed to ensure the timers correctly detected the fall of each animal and no animal cheated by hanging onto the rod. Mice participated in six trials each day for three consecutive days and were then tested on the fourth day. All mice had two training trials followed by a break, before the final trial. A total of seven mice were tested for each group. The heterozygous B2-ablated mice showed no difference compared with the wild-type mice and were used as a control together with the wild-type mice.

Data Analysis

The results were represented as average ± SE. Statistical analyses were used as described below: A two-way analysis of variance (ANOVA) followed by the Bonferroni test was carried out for motor coordination studies; Spearman correlation analysis was used to characterize the relationship between the facial neuron protrusion and the development of hydrocephalus in various NMHC II-B mutant mouse lines. Two-tailed Student's *t* test was used to compare the results between two groups.

RESULTS

Quantification and Tissue Distribution of Inserted Transcripts

We have previously reported that both the B1- and B2-inserted isoforms of NMHC II-B are only expressed in neuronal tissues in humans and chickens, although recently there is some disagreement about this finding in mice (Minovitsky *et al*., 2005). We, therefore, analyzed the expression of inserted NMHC II-B in various adult mouse tissues using RT-PCR. Figure 1A shows the schematic diagram of NMHC II-B and the location of the primers used in our RT-PCR analyses. Both the B1- and B2-inserted NMHC II-B were detected in neuronal tissues, including the brain (cerebrum, cerebellum, and brain stem), spinal cord, and eye, and no inserted isoforms were detected in any nonneuronal tissues tested in this analysis (Figure 1B).

Four isoforms of NMHC II-B are expressed in adult mouse brains resulting from the inclusion and/or exclusion of the alternatively spliced exons B1 and B2. These are a B1 single-inserted isoform, a B2 single-inserted isoform, and B1 and B2 double-inserted as well as a noninserted isoform of NMHC II-B. The majority of the NMHC II-B transcripts in the brain stem and spinal cord contain the alternative insert(s), and one-half of the total NMHC II-B transcripts contained both the B1 and B2 exons (Table 1). In the mouse cerebrum however, the majority of the NMHC II-B transcripts did not contain the alternative inserts. In the mouse cerebellum, ~40% of the total NMHC II-B is the B2-inserted isoform (Figure 1B, lane 10, and Table 1). These results suggest that inclusion of the B1 or B2 alternative exon is regulated by different mechanisms in different regions of the brain.

We next examined E12.5 (Figure 1C) and E16.5 mouse brains and spinal cords for the presence of alternative isoforms of NMHC II-B. At both E12.5 and E16.5, only the B1-inserted isoform, but not the B2-inserted isoform, was detected in the embryonic brain and spinal cord. However, compared with the noninserted NMHC II-B, less than 1% of the NMHC II-B was B1 inserted.

Generation of Insert-ablated NMHC II-B Mice

To explore the physiological function of the two alternatively spliced, neuron-specific isoforms of NMHC II-B, we generated two different lines of insert-specifically ablated mice by replacing exon B1 and separately, exon B2 with a floxed Neo^r cassette using homologous recombination (Figure 2, A and B). The former mice were designated as $B^{\Delta B1N}/B^{\Delta B1N}$ and the latter as $B^{\Delta B2N}/B^{\Delta B2N}$, where ΔB1 and ΔB2 signify the deleted exon and N signifies the presence of Neo^r in the targeted allele. The presence of the Neo^r cassette in the targeted allele resulted in decreased expression of total NMHC II-B in both $B^{\Delta B1N}/B^{\Delta B1N}$ (Figure 3A) and $B^{\Delta B2N}/B^{\Delta B2N}$ mice (Figure 3B). Quantification of the immunoblots showed that only 24 ± 4% (n = 8) of NMHC II-B is expressed in $B^{\Delta B1N}/B^{\Delta B1N}$ mice compared with wild-type mice, and 25 ± 4% (n = 5) of NMHC II-B is expressed in $B^{\Delta B2N}/B^{\Delta B2N}$ mice. A Student's *t* test, comparing NMHC II-B expression in $B^{\Delta B1N}/B^{\Delta B1N}$ mice with the $B^{\Delta B2N}/B^{\Delta B2N}$ mice, showed a lack of significant difference ($p = 0.83$). Removal of the floxed Neo^r cassette from the targeted alleles by crossing $B^{\Delta B1N}/B^{\Delta B1N}$ and, separately, $B^{\Delta B2N}/B^{\Delta B2N}$ mice with transgenic mice expressing Cre-recombinase under control of the cytomegalovirus (CMV) promoter generated $B^{\Delta B1}/B^{\Delta B1}$and $B^{\Delta B2}/B^{\Delta B2}$ mice, respectively, and restored protein expression of insert-deleted NMHC II-B to wild-type levels (Figure 3, C and D). For each construct, two different clones of the targeted embryonic stem cells were injected into blastocysts. Each of them was transmitted to the germline, and each showed the same phenotype for a given deleted exon. No abnormalities were observed in any of the heterozygous mice. Approximately 6% of the $B^{\Delta B1N}/B^{\Delta B1N}$ mice die by 3 wk after birth because of progressive overt hydrocephalus, but all of the $B^{\Delta B1}/B^{\Delta B1}$ and the B2 insert-ablated mice ($B^{\Delta B2N}/B^{\Delta B2N}$ and $B^{\Delta B2}/B^{\Delta B2}$) survive to adulthood.

Abnormal Migration of Facial Neurons

All of the $B^{\Delta B1N}/B^{\Delta B1N}$ mice had facial neurons that migrated abnormally. Instead of localizing to the lateral ventral region of the medulla underneath the pial surface, some B1 insert-ablated facial neurons abnormally protruded into the fourth ventricle (Figure 4, D and F, arrow). During embryonic development, facial neurons originate from the neuroepithelium on both sides of the neural tube between E10 and E12. These cells, which first migrate laterally and posteriorly, independently of glial cells, then migrate ventrally along the glial fibers to their final destination. By the end of their migration, they form two separate groups on the left and right side of the brain stem. However, in $B^{\Delta B1N}/B^{\Delta B1N}$

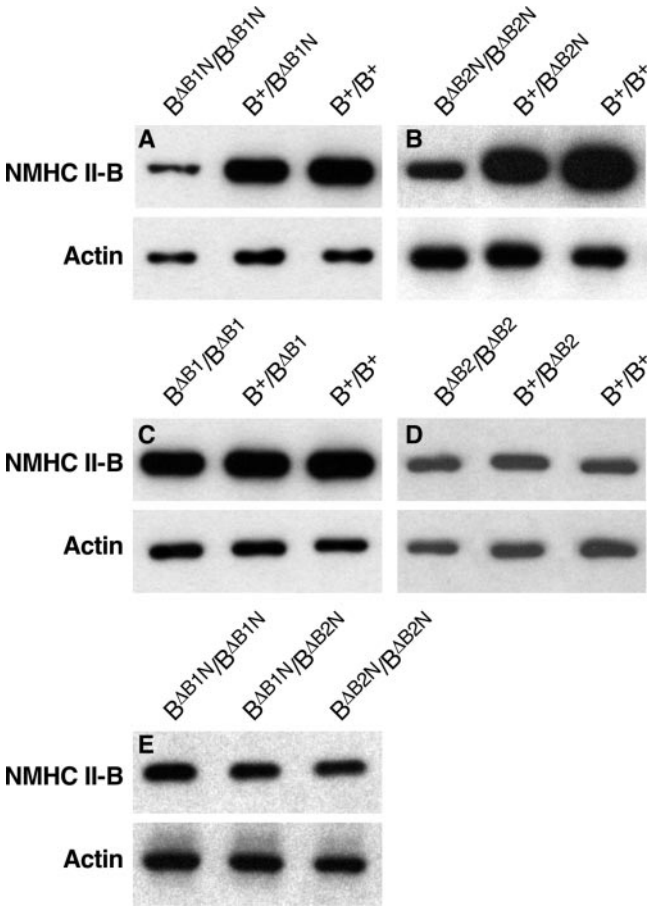

Figure 3. Immunoblot analyses of NMHC II-B expression of mouse brain extracts. (A) In the presence of the Neo^r cassette, the heterozygous ($B^+/B^{\Delta B1N}$) and homozygous ($B^{\Delta B1N}/B^{\Delta B1N}$) B1-ablated mice show a reduced amount of NMHC II-B expression compared with their wild-type littermates (B^+/B^+). (B) In the presence of Neo^r, the heterozygous ($B^+/B^{\Delta B2N}$) and homozygous ($B^{\Delta B2N}/B^{\Delta B2N}$) B2-ablated mice also show a reduced amount of NMHC II-B expression compared with their wild-type littermates (B^+/B^+). (C) After the removal of Neo^r from the targeted alleles, the heterozygous ($B^+/B^{\Delta B1}$) and homozygous ($B^{\Delta B1}/B^{\Delta B1}$) B1-ablated mice showed the same amount of NMHC II-B expression as their wild-type littermates (B^+/B^+). (D) The heterozygous ($B^+/B^{\Delta B2}$) and homozygous ($B^{\Delta B2}/B^{\Delta B2}$) B2-ablated mice also showed the same amount of NMHC II-B expression as their wild-type littermates (B^+/B^+) after the removal of Neo^r from the targeted alleles. (E) Littermates of $B^{\Delta B1N}/B^{\Delta B1N}$, $B^{\Delta B2N}/B^{\Delta B2N}$, and $B^{\Delta B1N}/B^{\Delta B2N}$ generated by crossing $B^{\Delta B1N}/B^{\Delta B2N}$ with $B^{\Delta B1N}/B^{\Delta B2N}$ mice showed the same amount of NMHC II-B expression. NMHC II-B was detected using an antibody to the C-terminal sequence. Actin was used as a loading control in all these analyses.

mice, some of the B1-ablated facial neurons migrated into the fourth ventricle and formed a single group of cells (Figure 4, D and F, arrow). To further understand how the deletion of the B1 insert led to the abnormal protrusion of the facial neurons into the fourth ventricle, we analyzed $B^{\Delta B1N}/B^{\Delta B1N}$ mice at E10.5, the time that facial neurons are just beginning to be generated. Figure 4A shows migrating facial neurons in a sagittal section of a wild-type mouse brain. Note that the facial neurons are distributed as a relatively thin stream under the neuroepithelial cells and that the ventricular surface lining the future fourth ventricle is intact (Figure 4A). In contrast, in the $B^{\Delta B1N}/B^{\Delta B1N}$ mice, the facial neurons have accumulated and are bunched up near the ventricular surface, which is disrupted just above the accumulated neurons (Figure 4B, black arrows). Indeed, some of the migrating neurons have begun to protrude into the ventricle. Compared with the mutant neurons, the wild-type neurons have clearly migrated more posteriorly. Of note and as shown in Figure 4B, only the migrating facial neurons near the ventricular surface and not the neuroepithelial cells are protruding into the fourth ventricle (Figure 4D). Interestingly, the facial neurons that are most distal from the ventricular surface align normally and continue to migrate toward their final destination. This suggests that there is no abnormality in the neuronal signaling affecting directional migration with respect to these neurons. Indeed, some of the facial neurons in $B^{\Delta B1N}/B^{\Delta B1N}$ mice do complete their migration and localize in their normal position (Figure 4H) as seen in all wild-type mice (Figure 4G). However, the number of facial neurons at their normal destination is significantly diminished in $B^{\Delta B1N}/B^{\Delta B1N}$ mice (Figure 4H) compared with wild-type littermates (Figure 4G) consistent with abnormal protrusion of ~50% of the $B^{\Delta B1N}/B^{\Delta B1N}$ facial neurons into the fourth ventricle (Figure 4F). At E14.5 the average number of facial neurons/5-μm section in wild-type mice reaching their final, normal destination was 240 $\pm$ 35. None of the facial neurons mismigrated. In contrast, only 120 $\pm$ 19 facial neurons reached their normal destination in $B^{\Delta B1N}/B^{\Delta B1N}$ mice. At E16.5, the numbers were 208 $\pm$ 30 for wild-type mice and 96 $\pm$ 16 for $B^{\Delta B1N}/B^{\Delta B1N}$ mice. Thus, there is a significant decrease in normally migrating neurons in the $B^{\Delta B1N}/B^{\Delta B1N}$ mice compared with wild-type mice (Student's t test, $p < 0.0001$, $n = 4$ mice for each group; see *Materials and Methods* for details). All of the $B^{\Delta B1N}/B^{\Delta B1N}$ mice analyzed in this study (more then 10 mice) showed the abnormal protrusion of facial neurons into the fourth ventricle. Importantly, these abnormalities were not seen in $B^{\Delta B1}/B^{\Delta B1}$ mice after removal of the Neo^r cassette and restoration of normal amounts of NMHC II-B expression, despite absence of the B1 insert. These results suggested that either the B1 insert was dispensable and the defects seen in $B^{\Delta B1N}/B^{\Delta B1N}$ mice were solely due to the reduced expression of total NMHC II-B or that the role of the B1-inserted isoform could be compensated for by the increased expression of noninserted NMHC II-B.

To clarify this question, we compared the $B^{\Delta B1N}/B^{\Delta B1N}$ mice with the $B^{\Delta B2N}/B^{\Delta B2N}$ mice. As noted above, both of these mouse lines showed approximately the same degree of reduction in total NHMC II-B expression due to the presence of the Neo^r cassette (Figure 3, A and B). However, none of the $B^{\Delta B2N}/B^{\Delta B2N}$ mice showed abnormal migration of their facial neurons. We therefore generated $B^{\Delta B1N}/B^{\Delta B2N}$ mice and crossed these mice with each other to produce $B^{\Delta B1N}/B^{\Delta B1N}$, $B^{\Delta B1N}/B^{\Delta B2N}$, and $B^{\Delta B2N}/B^{\Delta B2N}$ offspring that allowed us to directly compare these three genotypes from the same litter. Each of these mice showed the same level of total NMHC II-B expression (Figure 3E), but only the $B^{\Delta B1N}/B^{\Delta B1N}$ mice consistently had facial neurons that migrated abnormally. None of the $B^{\Delta B1N}/B^{\Delta B2N}$ and $B^{\Delta B2N}/B^{\Delta B2N}$ mice showed abnormalities in facial neuron migration. This suggests that one copy of the B1 insert is sufficient to prevent this abnormality in mice, which express 25% of the normal amount of NMHC II-B. These results demonstrated that deletion of the B1 insert itself contributed to the abnormal migration of facial neurons and that decreased expression of NMHC II-B alone is not the cause of these defects in $B^{\Delta B1N}/B^{\Delta B1N}$ mice.

Next, to further reduce the expression of NMHC II-B, we generated $B^{\Delta B1N}/B^-$ and $B^{\Delta B2N}/B^-$ mice by crossing the $B^{\Delta B1N}/B^{\Delta B1N}$ or the $B^{\Delta B2N}/B^{\Delta B2N}$ mice with heterozygous NMHC II-B ablated mice (B^+/B^-). This results in a further

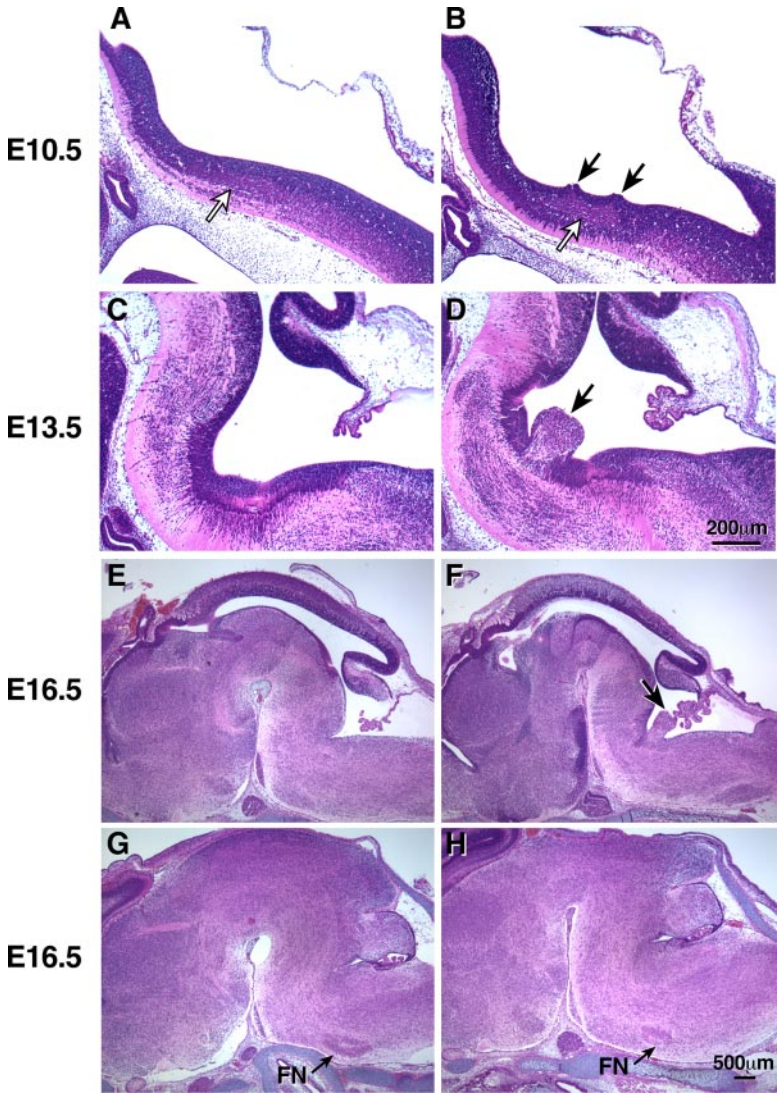

Figure 4. Impaired migration of facial neurons in $B^{\Delta B1N}/B^{\Delta B1N}$ mice. (A and B) H&E staining of sagittal sections of embryonic mouse brains at E10.5 show that the migrating facial neurons in wild-type mice (B^{+}/B^{+}) form a well organized thin stream under the neuroepithlial cells parallel to the ventricular surface (A, white arrow). In $B^{\Delta B1N}/B^{\Delta B1N}$ mice, the migrating facial neurons accumulate in one place (B, white arrow). Some of the $B^{\Delta B1N}/B^{\Delta B1N}$ facial neurons are oriented perpendicularly to the ventricular surface and are beginning to protrude into the future fourth ventricle through the ependymal layer (B, black arrows). The most distal facial neurons, however, are still oriented normally as in wild-type mice. (C and D) Sagittal sections of embryonic brains near the midline at E13.5, a time when the facial neurons have almost completed their migration, show abnormal protrusion of facial neurons into the fourth ventricle in $B^{\Delta B1N}/B^{\Delta B1N}$ mice (D, arrow) compared with wild-type (C). (E–H) Sagittal sections of E16.5 mouse brains in the middle (E and F) and lateral (G and H) region of the brain show protrusion of facial neurons (F, arrow) and reduced numbers of facial neurons (H, arrow) at their normal destination in $B^{\Delta B1N}/B^{\Delta B1N}$ mice compared with the wild-type littermates (E and G). At least five mice from each genotype were analyzed.

decrease in NMHC II-B expression to ~12% of the normal amount and leads to the development of facial neuron protrusion in both lines. This result indicates that the presence of the B1 insert cannot prevent the abnormal migration of the facial neurons once the amount of NMHC II-B is 12% or less (e.g., $B^{\Delta B2N}/B^{-}$ mice). Therefore, the inclusion of the B1-insert becomes critical for facial neuron migration when NMHC II-B expression is ~25% of the normal amount.

The abnormal migration of facial neurons has also been reported in NMHC II-B ablated mice and in mice with a single amino acid mutation in NMHC II-B (R709C) together with hypomorphic expression of the mutant II-B (Ma *et al.*, 2004). This particular mutation results in a decrease in the actin-activated MgATPase activity as well as loss of in vitro motility of HMM II-B (Kim *et al.*, 2005). Thus, facial neuron migration seems to correlate with both the quantity and quality of NMHC II-B. Table 2 summarizes the results from various mouse genotypes generated with respect to the abnormal protrusion of facial neurons into the fourth ventricle. To understand the determining factors underlying the abnormal migration of facial neurons in the various genotypes listed in Table 2, we introduced a hypothetical index value, the "total activity of myosin II-B." This value is defined as the

Table 2. Association of mouse phenotype and theoretical total ATPase activity

Genotype	Hydrocephalus (score[a])	Facial protrusion (score[a])	Total ATPase activity (%)[b]
$B^{\Delta B1N}/B^{\Delta B1N}$	Yes (2)	Yes (2)	19
$B^{\Delta B2N}/B^{\Delta B2N}$	No (0)	No (0)	25
$B^{\Delta B1N}/B^{\Delta B2N}$	No (0)	No (0)	22
$B^{\Delta B1N}/B^{-}$	Yes (3)	Yes (3)	10
$B^{\Delta B2N}/B^{-}$	Yes (3)	Yes (3)	12
$B^{\Delta B1}/B^{\Delta B1}$	No (0)	No (0)	76
$B^{\Delta B2}/B^{\Delta B2}$	No (0)	No (0)	100
B^{-}/B^{-}	Yes (4)	Yes (2)	0
B^{CN}/B^{CN}	Yes (4)	Yes (4)	8
B^{+}/B^{+} (wild type)	No (0)	No (0)	100

[a] Score is from 0 to 4, with 4 being most severely affected.

[b] Relative content of NMHC II-B times actin-activated MgATPase activity of HMM II-B. B1-inserted and noninserted ATPase activity is from Pato *et al.* (1996); R709C ATPase activity is from Kim *et al.* (2005). B2 insert is not expressed during embryonic stage, therefore $B^{\Delta B2}$ activity is same as wild type.

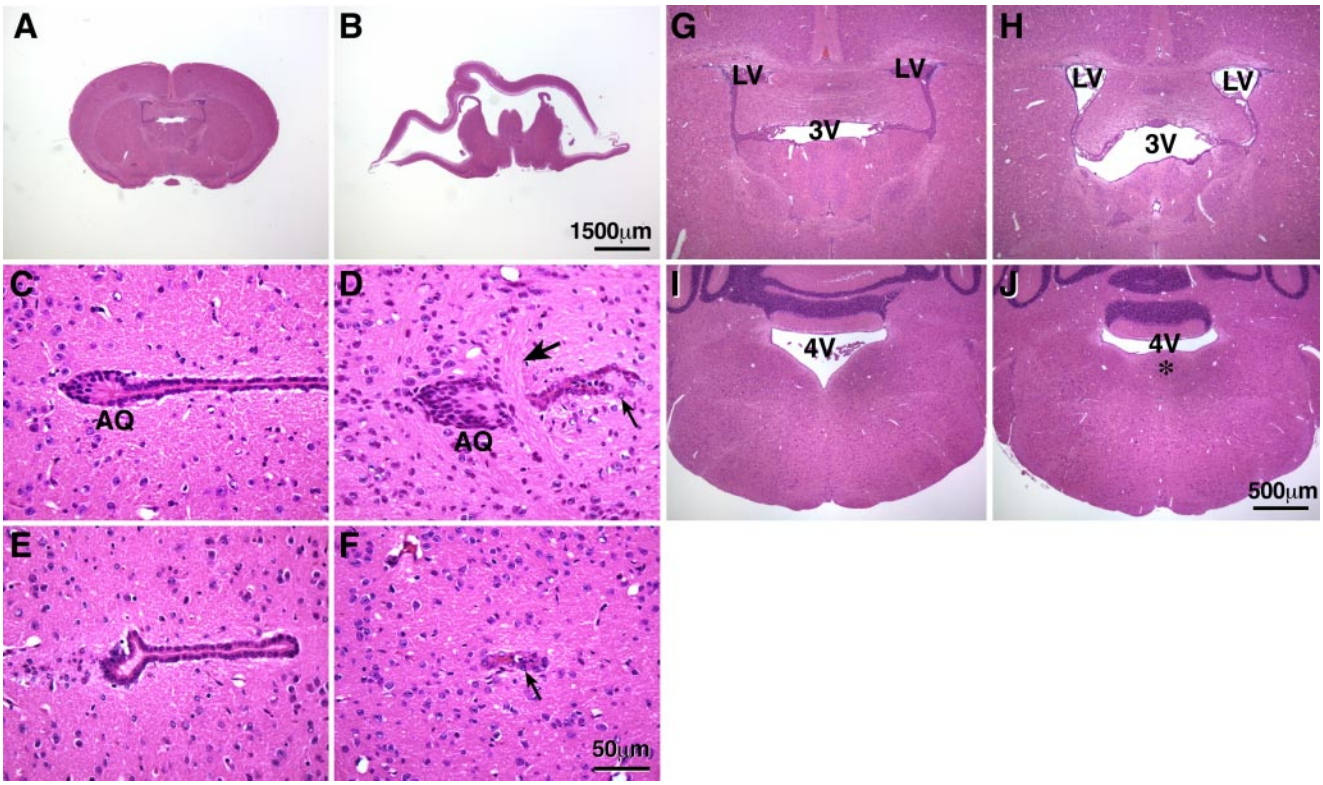

Figure 5. Development of hydrocephalus in $B^{\Delta B1N}/B^{\Delta B1N}$ mice. (A and B) H&E staining of coronal sections of mouse brains at P21 shows that, as a result of severe hydrocephalus in the $B^{\Delta B1N}/B^{\Delta B1N}$ mouse, the brain is massively disrupted (B) compared with the wild-type littermate (A). (C–F) Coronal sections of P21 mouse brains show the region around the aqueduct of Sylvius (C, AQ). In the wild-type mouse, the aqueduct of Sylvius is surrounded by an intact layer of ependymal cells (C and E). However, in $B^{\Delta B1N}/B^{\Delta B1N}$ mice, commissural fibers run across the aqueduct (D, large arrow), disrupting the ependymal layer (D and F, small arrow), and the lumen of the aqueduct is completely blocked (F). (G–J) H&E staining of coronal sections of mouse brains shows enlarged lateral and third ventricles in $B^{\Delta B1N}/B^{\Delta B1N}$ mice (panel H, LV and 3V) compared with wild-type littermates (G). Abnormal protrusion of the facial neurons into the fourth ventricle (4V) is observed in $B^{\Delta B1N}/B^{\Delta B1N}$ mice (J, *), which is not seen in the wild-type littermate (I).

relative content of NMHC II-B times the in vitro actin-activated MgATPase activity of baculovirus-expressed HMM II-B relative to that of B1-inserted HMM II-B. For wild-type mice, this index value is arbitrarily set as 100%, and for the different mutant mice, this value is expressed as a percentage relative to the wild-type mice. For simplicity, we assume that the facial neurons contain only the B1-inserted isofoms of NMHC II-B. The calculated values are listed in Table 2 and show that a total ATPase activity of 19% or less is accompanied by the abnormal migration of facial neurons (see *Discussion*).

Development of Hydrocephalus in $B^{\Delta B1N}/B^{\Delta B1N}$ Mice

In addition to abnormalities in facial neuron migration, the $B^{\Delta B1N}/B^{\Delta B1N}$ mice developed hydrocephalus. Approximately 6% (9 of 146) of the $B^{\Delta B1N}/B^{\Delta B1N}$ mice developed a severe progressive overt hydrocephalus and died at 3 wk after the birth. Figure 5B shows a coronal section of the brain from one of these mice. The brain is massively distorted due to the hydrocephalus, and only a very thin layer of the cortex remains. A control section from a wild-type littermate is shown in Figure 5A. Scanning of serial brain sections from $B^{\Delta B1N}/B^{\Delta B1N}$ mice showed that the cerebral ventricles, including the lateral and third ventricles were all extensively dilated. At the region of the aqueduct of the Sylvius, commissural fibers abnormally cross through the aqueduct (Figure 5D, arrow). The normal aqueduct is surrounded by an intact single cell layer of ependymal cells (Figure 5, C and E), and this layer is disrupted, and the lumen of the aqueduct is blocked in $B^{\Delta B1N}/B^{\Delta B1N}$ mice (Figure 5, D and F, arrow). These defects in the aqueduct of the Sylvius are sufficient to result in a progressive hydrocephalus in 6% of these $B^{\Delta B1N}/B^{\Delta B1N}$ mice. In contrast, the majority (94%) of $B^{\Delta B1N}/B^{\Delta B1N}$ mice survived to adulthood and showed no sign of an overt hydrocephalus. However, all of these mice showed evidence of hydrocephalus after sectioning of the brain, which was manifested as the enlargement of cerebral ventricles, including the lateral and third ventricles (Figure 5H), compared with the wild-type mice (Figure 5G). Except for the abnormal protrusion of the facial neurons into the fourth ventricle, no other obvious defects were seen in these mice (Figure 5J). Similar to the abnormal migration of facial neurons, hydrocephalus is not seen in B2-ablated mice or in B1-ablated mice in which wild-type level of NMHC II-B expression was restored. For the convenience of statistical analysis, we scored the severity of hydrocephalus and facial neuron protrusion from 0 to 4, where 0 means no hydrocephalus or no facial neuron protrusion, and 4 means the most severe condition such as in the B^{CN}/B^{CN} mice (Table 2). A Spearman correlation analysis showed a positive correlation between protrusion of the facial neurons into the fourth ventricle and the development of hydrocephalus in these mice (Spearman $r = 0.9196$, $p = 0.0003$; see *Discussion*).

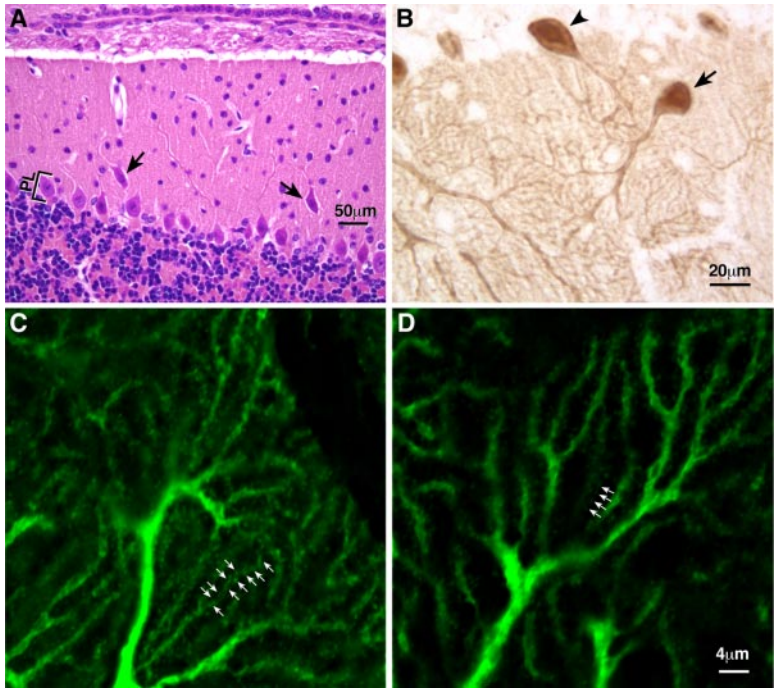

Figure 6. Abnormalities in the cerebellar Purkinje cell development in B2 insert-ablated mice. (A) H&E staining of a sagittal section of adult B2 insert-ablated mouse cerebellum shows misplacement of some of the cerebellar Purkinje cells (arrows) from the Purkinje cell layer (PL) to the molecular layer. (B) Immunohistochemical staining of a sagittal section of B2-ablated mouse cerebellum using antibodies against calbindin shows an abnormal orientation of the dendritic tree of some Purkinje cells (arrow) compared with their normal perpendicular orientation (arrowhead). (C and D) Immunofluorescence confocal images using antibodies against calbindin show a decreased number of dendritic branches and spines (arrows) in the Purkinje cells of a B2 insert-ablated mouse (D) compared with a wild-type littermate (C).

Abnormalities in Cerebellar Purkinje Cells in the B2 Insert-ablated Mice

Unlike the $B^{\Delta B1N}/B^{\Delta B1N}$ mice, none of the $B^{\Delta B2N}/B^{\Delta B2N}$ mice developed abnormalities in facial neuron migration or hydrocephalus. However, $B^{\Delta B2N}/B^{\Delta B2N}$ mice showed abnormalities in the development of the cerebellar Purkinje cells. The cell bodies of a small percentage of the Purkinje cells were consistently dissociated from the cerebellar Purkinje cell layer and were ectopically located in the molecular layer (Figure 6A, arrows). Immunohistochemical staining of parasagittal sections of the adult mouse cerebellum using an antibody against calbindin, which specifically stains Purkinje cells, revealed an abnormal orientation of the dendritic tree of a small number of the $B^{\Delta B2N}/B^{\Delta B2N}$ Purkinje cells (Figure 6B, arrow). Normally, Purkinje cells are oriented perpendicularly to the surface of the cerebellar cortex (Figure 6B, arrowhead). Importantly, immunofluorescence microscopy of calbindin staining further demonstrated that almost all of the $B^{\Delta B2N}/B^{\Delta B2N}$ Purkinje cells showed a marked decrease in branches and dendritic spines (Figure 6D) compared with the wild-type cells (Figure 6C). Branches were counted as the number of dendritic branches crossing lines perpendicular to the orientation of the dendritic arbors in confocal images stained with calbindin. The spines were counted on an individual branch. On average, 4.6 ± 0.12 and 3.8 ± 0.17 branches crossed a 10-μm-long line in B^+/B^+ and $B^{\Delta B2N}/B^{\Delta B2N}$ mice, respectively (Student's t test, $p < 0.005$, $n = 5$ mice in each group). The average spine number was 1.25 ± 0.04 and $0.79 \pm 0.05/\mu$m length of dendrites for B^+/B^+ and $B^{\Delta B2N}/B^{\Delta B2N}$ mice, respectively (Student's t test, $p < 0.0001$, $n = 5$ mice in each group). These defects were not dependent on the amount of total NMHC II-B expression because $B^{\Delta B2}/B^{\Delta B2}$ mice showed the exact same phenotypes as the hypomorphic $B^{\Delta B2N}/B^{\Delta B2N}$ mice. In contrast, the $B^{\Delta B1N}/B^{\Delta B1N}$ and $B^{\Delta B1}/B^{\Delta B1}$ mice showed no defects in the cerebellar Purkinje cells. These results demonstrate that B2-inserted NMHC II-B plays a unique role in cerebellar Purkinje cell development. This unique function cannot be compensated for by other isoforms of NMHC II-B (i.e., NMHC II-B containing the B1 insert alone or NMHC II-B that lacks the B2 exon).

Temporal and Spatial Expression of the B2-inserted NMHC II-B in the Developing Mouse Brain

To better understand the function and distribution of B2-inserted NMHC II-B, we generated peptide antibodies specifically against the 21 amino acids making up the entire B2 insertion. Immunoblot analysis shows that the antibodies detect B2-inserted NMHC II-B (Figure 7A, top lane) in wild-type and heterozygous cerebellar extracts (Figure 7A, lanes 1, 2, and 6). As expected, no signal is seen when the B2 insert is ablated. In contrast, total NMHC II-B (noninserted, and when present, inserted) is detected in each of the extracts using antibodies to the C-terminal end of the molecule (middle row). The lung extract is a negative control, because this tissue is devoid of the inserted isoform. Having ascertained the specificity of the antibodies, we used them to localize the B2-inserted isoform in wild-type cerebellums of adult mice using immunohistochemistry. Figure 7B shows that the antibody stained cerebellar Purkinje cells in wild-type (Figure 7B), but not in $B^{\Delta B2N}/B^{\Delta B2N}$ mouse brains (Figure 7C, arrows).

Figure 8 uses confocal immunofluorescence microscopy to compare the staining of parasagittal sections of a P10 mouse cerebellum using antibodies raised to the C-terminal sequence of NMHC II-B, which detects both the inserted and noninserted isoforms of NMHC II-B (Figure 8A, red) with staining of serial sections using antibodies that specifically recognize the B2-inserted isoform (Figure 8B, red). Both sections are also costained with antibodies to glial fibrillary acidic protein (GFAP), which is a marker for glial cells (green). These panels show that the B2-inserted isoform of NMHC II-B is confined to the Purkinje cells (Figure 8B) but that noninserted NMHC II-B is also present in glial fibers (Figure 8A, greenish yellow) as well as other neurons in the cerebellum (Figure 8A, red). Figure 8C shows costaining of similar serial sections with C-terminal antibodies to total NMHC II-B and antibodies to calbindin, a marker for Purkinje

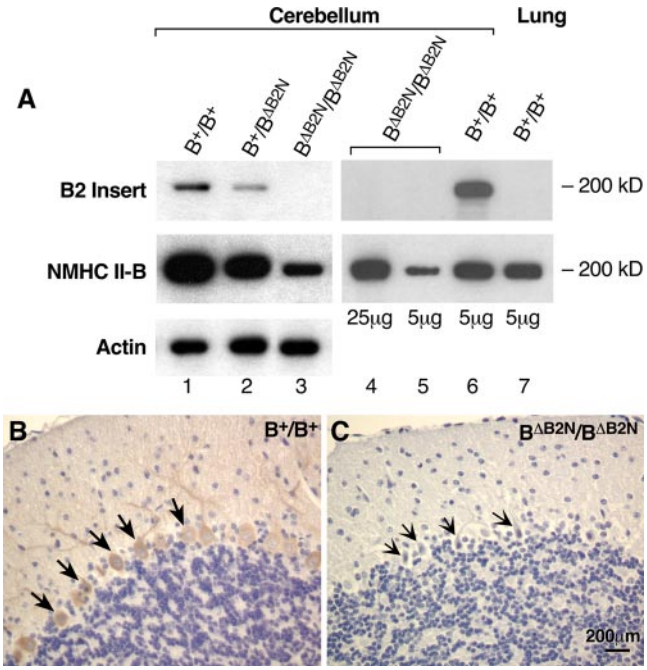

Figure 7. Specificity of peptide antibodies against the B2-inserted NMHC II-B. (A) Immunoblot analysis of protein extracts prepared from the cerebellum and lung demonstrate that the B2 insert-specific antibody reacts only with B2-inserted NMHC II-B. Lanes 1, 2, and 3 are immunoblots of cerebellar extracts from wild-type, heterozygous and homozygous mice, demonstrating the specificity of the antibody for the B2 insert. Actin was used as a loading control. Lanes 4 and 5 show different loadings of the cerebellar extracts for B2-ablated mice and include an extract from lung tissue as a negative control (lane7). (B and C) Immunohistochemical staining of sagittal sections of mouse cerebellum demonstrate specific staining by the B2 antibody in wild-type cerebellar Purkinje cells (B, brown color, arrows), but no staining is detected in B2 insert-ablated mouse cerebellum (C, arrows).

cells. Note the costaining of the Purkinje cells (yellow) and the presence of NMHC II-B in other cells in this area (red). Figure 8D confirms that the B2-inserted isoform, unlike the noninserted isoform, is only present in the Purkinje cells of the cerebellum (Figure 8D, yellow, and lack of red in surrounding cells as seen in Figure 8C).

Figure 9A shows the results of RT-PCR to determine the timing for the initiation of B2 expression during mouse cerebellar development. The figure shows that the insert is first expressed 7 or 8 d after birth. Relative to the noninserted NMHC II-B, the B2-inserted isoform increases between P8 to P14 and remains essentially unchanged through P56. These results are consistent with immunofluorescence microscopic staining of the developing cerebellum between P7 and P14 using B2 insert-specific antibodies (Figure 9, B and C). Expression of the B2-inserted NHMC II-B keeps increasing between P14 and P21 (cf. Figure 9, C and D). Figure 9E, which is a higher magnification study, provides evidence that the B2 insert-specific antibodies stain cerebellar Purkinje cells with a punctated pattern. Of note is that some of the B2-inserted isoform of NMHC II-B (green) colocalizes with phalloidin-actin (Figure 9E, red) in the spines of cerebellar dendrites (yellow in Figure 9E, arrows). Both the temporal and regional distribution of the B2 insert is consistent with its function in postnatal development of the cerebellar Purkinje cells.

Impaired Balance in B2-ablated Mice

Consistent with defects in cerebellar Purkinje cells, both the $B^{\Delta B2N}/B^{\Delta B2N}$ (hypomorphic) and $B^{\Delta B2}/B^{\Delta B2}$ (nonhypomorphic) mice showed impaired motor coordination. The B2 insert-ablated mice showed a reduced ability to maintain their balance on a rotarod compared with their wild-type littermates ($p < 0.05$, two-way ANOVA, $n = 7$; Table 3). With three testing rates, 20, 32, and 40 rpm, no significant difference in ability to remain on the rod was found for the wild-type mice. However, the performance of the B2 insert-ablated mice depended on the rotation rate of the rod. At lower rates, the B2 insert-ablated mice showed no deficiency. With an increase of rotation speed,

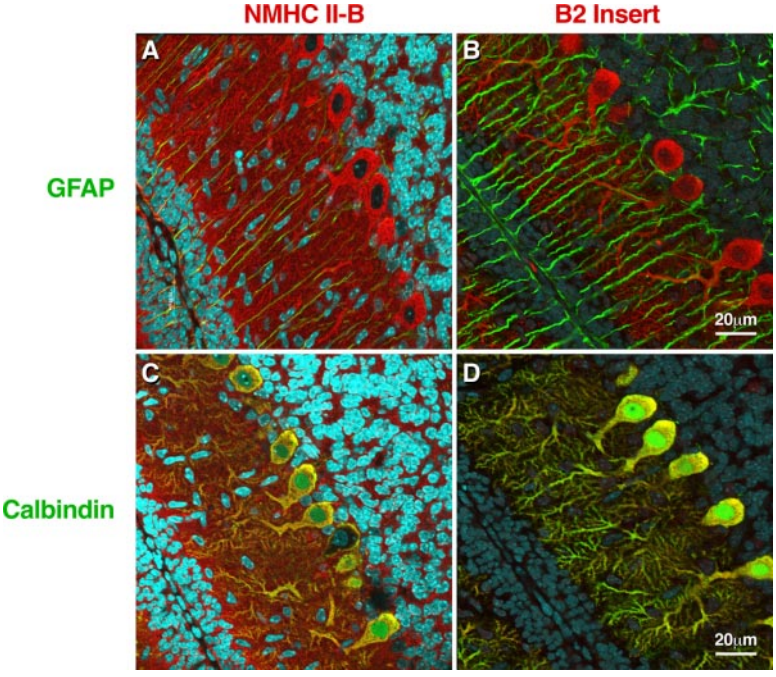

Figure 8. Immunofluorescence confocal images of mouse cerebellum at P10 using the indicated antibodies. (A) Costaining with antibodies for NMHC II-B (red) and glial-specific GFAP (green) shows that NMHC II-B is expressed in the Bergman glial fibers (yellow) as well as other cerebellar cells (red). (B) Costaining with antibodies specific for B2-inserted NMHC II-B (red) and GFAP (green) shows that the B2-inserted NMHC II-B does not costain with GFAP, indicating that B2-inserted NMHC II-B is not expressed in the Bergman glial cells and is confined to the Purkinje cells. (C) Costaining with antibodies for NMHC II-B (red) and the Purkinje cell-specific protein calbindin (green) shows that NMHC II-B and calbindin are both present in the Purkinje cells (yellow) but that NMHC-II-B is also present in other cells, too, such as granule cells (red). (D) Costaining with antibodies for B2-inserted NMHC II-B (red) and calbindin (green) shows that both proteins are confined to the Purkinje cells (yellow). Nuclei are stained with DAPI (blue).

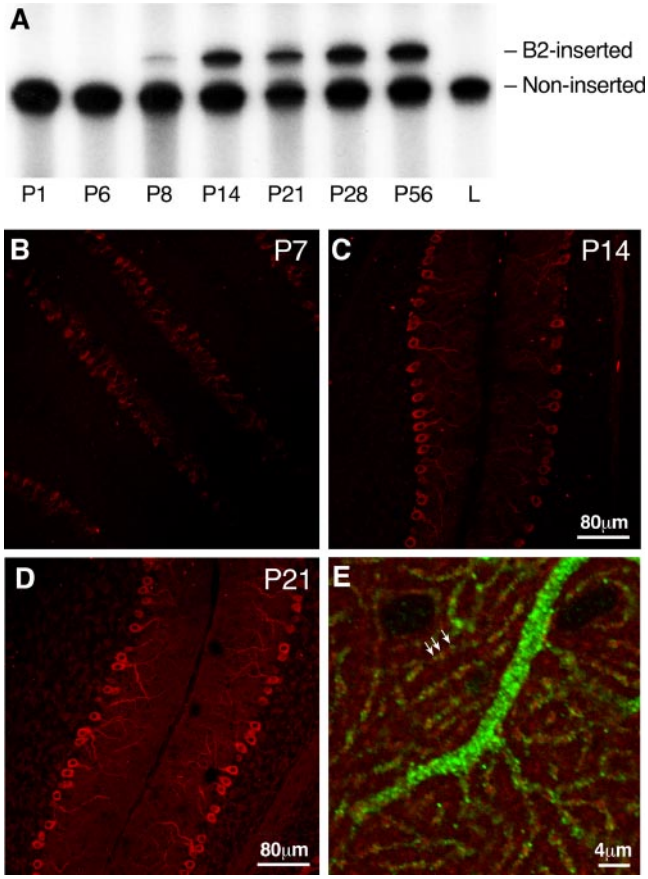

Figure 9. Temporal and regional expression of B2-inserted NMHC II-B in mouse cerebellum. (A) Autoradiogram after RT-PCR analysis of mRNA expression of B2-inserted NMHC II-B in wild-type mouse cerebellum during postnatal development. α-^{32}P-dCTP was incorporated during PCR. Note that mRNA encoding the B2-inserted NMHC II-B is not detected in mouse cerebellum at P6, but it is expressed at P8, increases thereafter, and is maintained during adulthood. Adult lung (L) was used as a negative control for inserted NMHC II-B. (B–D) Immunofluorescence confocal microscopy of developing mouse cerebellum using B2 insert-specific antibody shows that B2-inserted NMHC II-B is detected in cerebellar Purkinje cells at P7 (B, red). Increased staining is seen at P14 and P21 (C and D, red). (E) A sagittal section of mouse cerebellum at P14 costained with B2 insert-specific antibody (green) and rhodamine-phalloidin for F-actin (red). Both the B2 insert-specific antibody and rhodamine-phalloidin showed punctuate staining. Yellow indicates colocalization of B2-inserted NMHC II-B and actin, indicating the dendritic spines (arrows).

Table 3. Rotarod performance of the B2-ablated and control mice

Speed (rpm)	Time balanced on rotarod (s)		p value (Bonferroni post test)
	Control[a]	B2-ablated[b]	
20	54 ± 6	52 ± 6	>0.05
32	44 ± 6	41 ± 6	>0.05
40	53 ± 6	29 ± 4	<0.01

[a] Includes heterozygous and wild-type littermates.

[b] $p < 0.05$, statistically significant compared to control group (two-way ANOVA, n = 7).

their performance decreased. At 40 rpm, a significantly impaired performance was found in the B2 insert-ablated mice compared with their wild-type littermates ($p < 0.01$, Bonferroni post test; Table 3).

DISCUSSION

The present study demonstrates that the neuron-specific products of alternative splicing of NMHC II-B have different functions during mouse brain development. Whereas deletion of B1-inserted NMHC II-B results in abnormal migration of the facial neurons, deletion of the B2-inserted isoform leads to abnormalities in cerebellar development, particularly with respect to Purkinje cell localization and maturation. This latter defect is manifested by impaired motor activity in the B2 insert-deleted mice.

NMHC II-B Activity and Facial Neuron Migration

Replacing either the exon encoding the B1 insert or the B2 insert with floxed Neo^r results in an approximately 75% decrease in the expression of total NMHC II-B in homozygous mice. However, the presence of only 25% of the normal amount of NMHC II-B is sufficient to prevent abnormal migration of the facial neurons and hydrocephalus but only provided the B1 insert is still present. These abnormalities are not seen once the expression of total NMHC II-B is restored by removing the Neo^r cassette in the B1 insert-ablated mice, indicating the importance of decreased NMHC II-B expression in generating this defect. Therefore, both the inclusion of the B1 insert as well as the total amount of myosin II-B are involved in controlling normal migration of the facial neurons. Pato *et al*. (1996) demonstrated that B1-inserted HMM II-B shows an increased actin-activated MgATPase activity and ability to translocate actin filaments in vitro, compared with the noninserted isoform. We, therefore, postulated that proper migration of the facial neurons is dependent on myosin II-B activity in vivo and compared the theoretical total actin-activated MgATPase activity of HMM II-B isoforms among the various mutant and wild-type mice (Table 2). The data from Table 2 show that, when the total ATPase activity of myosin II-B is less than ~20% of wild type, there is an abnormality in facial neuron migration. Thus, a reduction in myosin II-B content and alteration of the isoform slow migration of the facial neurons and leads to the accumulation of facial neurons under the ventricular surface near their origin. As shown in Figure 4B, the accumulated mutant facial neurons protrude through the ventricular surface. Therefore, it is also possible that the cells lining the ventricular surface in $B^{\Delta B1N}/B^{\Delta B1N}$ mice have a weakening in their cell–cell adhesion.

Association of Abnormal Facial Neuron Migration with Hydrocephalus

To elucidate the physiological roles of NHMC II-B, we have generated a number of mouse lines affecting the gene encoding NMHC II-B (Tullio *et al*., 2001; Ma *et al*., 2004). A constant phenotype found in each of these mice is the development of hydrocephalus. In these mice, the development of hydrocephalus was always associated with an abnormal protrusion of facial neurons into the fourth ventricle. Indeed, the severity of hydrocephalus also seems to correlate with the severity of the abnormality in facial neuron migration. In mice with the R709C mutation, which expressed a decreased amount of the mutant NMHC II-B (B^{CN}/B^{CN}), a majority of the facial neurons protruded abnormally into the fourth ventricle, and all these mice developed a severe, overt hydrocephalus. In $B^{\Delta B1N}/B^{\Delta B1N}$ mice, a

relatively small number of facial neurons protruded. Accordingly, most of these mice developed a milder hydrocephalus. We, therefore, propose that abnormal protrusion of the facial neurons into the fourth ventricle contributes to the development of hydrocephalus seen in NMHC II-B mutant mice, and an increase in the number of protruding neurons contributes to the severity of hydrocephalus. Indeed, abnormality in facial neuron migration is the only brain defect observed in the B1 insert-ablated mice with decreased myosin expression. This is in contrast to the R709C hypomorphic mice, which show defects in the migration of cerebellar and pontine neurons in addition to facial neurons. It is possible that the protrusion of facial neurons into the fourth ventricle results in a disturbance in the normal laminar flow of the cerebrospinal fluid and partially blocks the entrance to the fourth ventricle.

Overt progressive hydrocephalus is usually accompanied by blockage of the aqueduct of the Sylvius as we have found in some of the $B^{\Delta B1N}/B^{\Delta B1N}$ mice. Blockage of the aqueduct of the Sylvius could accelerate the development of the hydrocephalus. However, this is usually not the cause but rather the effect of hydrocephalus (Raimondi *et al.*, 1976; Wagner *et al.*, 2003). In $B^{\Delta B1N}/B^{\Delta B1N}$ mice, development of the overt progressive hydrocephalus occurs around 2 wk after the birth. The protrusion of the facial neurons into the fourth ventricle is seen as early as E11.5. We therefore suggest that the initiation of the hydrocephalus is associated with abnormal protrusion of the facial neurons in all $B^{\Delta B1N}/B^{\Delta B1N}$ mice.

Role of the B2-inserted Isoform

In agreement with a previous report on the developing rat cerebellum, both the regional and temporal pattern of the B2 insert expression is similar in the developing mouse cerebellum (Miyazaki *et al.*, 2000). This insert seems to be required for normal maturation of cerebellar Purkinje cells, including the dendrites and dendritic spine formation. In the developing mouse cerebellum, the B2 insert appears 1 wk after birth and gradually increases during the next 2 wk, compatible with the maturation time course of the cerebellar Purkinje cells (Altman and Bayer, 1997). The predominant expression of the B2 insert in both developing and mature Purkinje cells further supports its importance in postnatal development of these cells. In addition, the punctate distribution and colocalization of B2-inserted NMHC II-B with actin, both of which are enriched in the dendritic spines (Matus, 2000, for actin localization), indicates a possible role in spine formation. These ideas were further supported by the finding that deletion of the B2 insert caused a reduction in the number of spines and dendritic branches associated with Purkinje cells (Figure 6D). Consistent with these ideas, the importance of NHMC II-B in the regulation of lamellopodia and filapodia formation was previously demonstrated in studies on NMHC II-B ablated neuronal growth cones (Bridgman *et al.*, 2001). In that case, ablation of NMHC II-B also caused abnormalities in actin organization and impaired normal growth cone shape and polarization.

Unlike B1-inserted NMHC II-B where the function of this isoform can be compensated for by increased expression of B1-ablated NMHC II-B, B2-inserted NMHC II-B plays a unique role in postnatal development of cerebellar Purkinje cells. Replacement of the B2-inserted isoform with B2-ablated NMHC II-B cannot rescue the abnormalities seen in B2 insert-ablated mice. These results suggest that the function of B2-inserted NMHC II-B may not simply rely on the ATPase activity of this myosin.

Brain is the organ where alternative splicing takes place most frequently. This may reflect the complexity of structure and function of the central nervous system (for review, see Grabowski and Black, 2001). Our study demonstrates that two alternatively spliced isoforms play distinct roles in different types of neuronal cells and shows that the proper regulation of alterative splicing of NMHC II-B is necessary for normal development of the mouse brain.

ACKNOWLEDGMENTS

We are particularly indebted to Drs. Shirley Bayer and Joseph Altman as well as to Mary Anne Conti, Yoshinobu Hara, and Jim Sellers for valuable comments on the manuscript. Drs. Chengyu Liu and Yubin Du (National Heart, Lung, and Blood Institute [NHLBI] Transgenic Core) and Dr. Christian A. Combs (NHLBI Light Microscopy Core) provided outstanding service and advice. Antoine Smith provided excellent technical assistance and Catherine Magruder's editorial assistance is also gratefully acknowledged. This research was supported by the Division of Intramural Research, NHLBI.

REFERENCES

Altman, J., and Bayer, S. A. (1997). Development of the Cerebellar System in Relation to Its Evolution, Structure, and Functions, Boca Raton, FL: CRC Press.

Babu, G. J., Loukianov, E., Loukianova, T., Pyne, G. J., Huke, S., Osol, G., Low, R. B., Paul, R. J., and Periasamy, M. (2001). Loss of SM-B myosin affects muscle shortening velocity and maximal force development. Nat. Cell Biol. *3*, 1025–1029.

Bao, J., Jana, S. S., and Adelstein, R. S. (2005). Vertebrate nonmuscle myosin II isoforms rescue small interfering RNA-induced defects in COS-7 cell cytokinesis. J. Biol. Chem. *280*, 19594–19599.

Bridgman, P. C., Dave, S., Asnes, C. F., Tullio, A. N., and Adelstein, R. S. (2001). Myosin IIB is required for growth cone motility. J. Neurosci. *21*, 6159–6169.

Chantler, P. D., and Wylie, S. R. (2003). Elucidation of the separate roles of myosins IIA and IIB during neurite outgrowth, adhesion and retraction. IEE Proc. Nanobiotechnol. *150*, 111–125.

Conti, M. A., Even-Ram, S., Liu, C., Yamada, K. M., and Adelstein, R. S. (2004). Defects in cell adhesion and the visceral endoderm following ablation of nonmuscle myosin heavy chain II-A in mice. J. Biol. Chem. *279*, 41263–41266.

De Lozanne, A., and Spudich, J. A. (1987). Disruption of the Dictyostelium myosin heavy chain gene by homologous recombination. Science *236*, 1086–1091.

Fiering, S., Epner, E., Robinson, K., Zhuang, Y., Telling, A., Hu, M., Martin, D. I., Enver, T., Ley, T. J., and Groudine, M. (1995). Targeted deletion of 5′ HS2 of the murine β-globin LCR reveals that it is not essential for proper regulation of the β-globin locus. Genes Dev. *9*, 2203–2213.

Golomb, E., Ma, X., Jana, S. S., Preston, Y. A., Kawamoto, S., Shoham, N. G., Goldin, E., Conti, M. A., Sellers, J. R., and Adelstein, R. S. (2004). Identification and characterization of nonmuscle myosin II-C, a new member of the myosin II family. J. Biol. Chem. *279*, 2800–2808.

Grabowski, P. J., and Black, D. L. (2001). Alternative RNA splicing in the nervous system. Prog. Neurobiol. *65*, 289–308.

Guo, N., and Kawamoto, S. (2000). An intronic downstream enhancer promotes 3′ splice site usage of a neural cell-specific exon. J. Biol. Chem. *275*, 33641–33649.

Itoh, K., and Adelstein, R. S. (1995). Neuronal cell expression of inserted isoforms of vertebrate nonmuscle myosin heavy chain II-B. J. Biol. Chem. *270*, 14533–14540.

Karagiannis, P., Babu, G. J., Periasamy, M., and Brozovich, F. V. (2003). The smooth muscle myosin seven amino acid heavy chain insert's kinetic role in the crossbridge cycle for mouse bladder. J. Physiol. *547*, 463–473.

Kelley, C. A., Takahashi, M., Yu, J. H., and Adelstein, R. S. (1993). An insert of seven amino acids confers functional differences between smooth muscle myosins from the intestines and vasculature. J. Biol. Chem. *268*, 12848–12854.

Kim, K.-Y., Kovacs, M., Kawamoto, S., Sellers, J. R., and Adelstein, R. S. (2005). Disease-associated mutations and alternative splicing alter the enzymatic and motile activity of nonmuscle myosins II-B and II-C. J. Biol. Chem. *280*, 22769–22775.

Kolega, J. (2003). Asymmetric distribution of myosin IIB in migrating endothelial cells is regulated by a rho-dependent kinase and contributes to tail retraction. Mol. Biol. Cell *14*, 4745–4757.

Lo, C. M., Buxton, D. B., Chua, G. C., Dembo, M., Adelstein, R. S., and Wang, Y. L. (2004). Nonmuscle myosin IIb is involved in the guidance of fibroblast migration. Mol. Biol. Cell *15*, 982–989.

Ma, X., Kawamoto, S., Hara, Y., and Adelstein, R. S. (2004). A point mutation in the motor domain of nonmuscle myosin II-B impairs migration of distinct groups of neurons. Mol. Biol. Cell *15*, 2568–2579.

Matus, A. (2000). Actin-based plasticity in dendritic spines. Science *290*, 754–758.

Minovitsky, S., Gee, S. L., Schokrpur, S., Dubchak, I., and Conboy, J. G. (2005). The splicing regulatory element, UGCAUG, is phylogenetically and spatially conserved in introns that flank tissue-specific alternative exons. Nucleic Acids Res. *33*, 714–724.

Meshel, A. S., Wei, Q., Adelstein, R. S., and Sheetz, M. P. (2005). Basic mechanism of three-dimensional collagen fibre transport by fibroblasts. Nat. Cell Biol. *7*, 157–164.

Meyers, E. N., Lewandoski, M., and Martin, G. R. (1998). An Fgf8 mutant allelic series generated by Cre- and Flp-mediated recombination. Nat. Genet. *18*, 136–141.

Miyazaki, T., Watanabe, M., Yamagishi, A., and Takahashi, M. (2000). B2 exon splicing of nonmuscle myosin heavy chain IIB is differently regulated in developing and adult rat brain. Neurosci. Res. *37*, 299–306.

Pato, M. D., Sellers, J. R., Preston, Y. A., Harvey, E. V., and Adelstein, R. S. (1996). Baculovirus expression of chicken nonmuscle heavy meromyosin II-B. Characterization of alternatively spliced isoforms. J. Biol. Chem. *271*, 2689–2695.

Phillips, C. L., Yamakawa, K., and Adelstein, R. S. (1995). Cloning of the cDNA encoding human nonmuscle myosin heavy chain-B and analysis of human tissues with isoform-specific antibodies. J. Muscle Res. Cell Motil. *16*, 379–389.

Raimondi, A. J., Clark, S. J., and McLone, D. G. (1976). Pathogenesis of aqueductal occlusion in congenital murine hydrocephalus. J. Neurosurg. *45*, 66–77.

Stamm, S., Ben-Ari, S., Rafalska, I., Tang, Y., Zhang, Z., Toiber, D., Thanaraj, T. A., and Soreq, H. (2005). Function of alternative splicing. Gene *344*, 1–20.

Svitkina, T. M., Verkhovsky, A. B., McQuade, K. M., and Borisy, G. G. (1997). Analysis of the actin-myosin II system in fish epidermal keratocytes: mechanism of cell body translocation. J. Cell Biol. *139*, 397–415.

Takahashi, M., Kawamoto, S., and Adelstein, R. S. (1992). Evidence for inserted sequences in the head region of nonmuscle myosin specific to the nervous system. Cloning of the cDNA encoding the myosin heavy chain-B isoform of vertebrate nonmuscle myosin. J. Biol. Chem. *267*, 17864–17871.

Takeda, K., Kishi, H., Ma, X., Yu, Z.-X., and Adelstein, R. S. (2003). Ablation and mutation of nonmuscle myosin heavy chain II-B results in a defect in cardiac myocyte cytokinesis. Circ. Res. *93*, 330–337.

Takeda, K., Yu, Z.-X., Qian, S., Chin, T. K., Adelstein, R. S., and Ferrans, V. J. (2000). Nonmuscle myosin II localizes to the Z-lines and intercalated discs of cardiac muscle and to the Z-lines of skeletal muscle. Cell Motil. Cytoskeleton *46*, 59–68.

Tullio, A. N., Bridgman, P. C., Tresser, N. J., Chan, C. C., Conti, M. A., Adelstein, R. S., and Hara, Y. (2001). Structural abnormalities develop in the brain after ablation of the gene encoding nonmuscle myosin II-B heavy chain. J. Comp. Neurol. *433*, 62–74.

Uren, D., *et al*. (2000). Gene dosage affects the cardiac and brain phenotype in nonmuscle myosin II-B-depleted mice. J. Clin. Investig. *105*, 663–671.

Wagner, C., Batiz, L. F., Rodriguez, S., Jimenez, A. J., Paez, P., Tome, M., Perez-Figares, J. M., and Rodriguez, E. M. (2003). Cellular mechanisms involved in the stenosis and obliteration of the cerebral aqueduct of hyh mutant mice developing congenital hydrocephalus. J. Neuropathol. Exp. Neurol. *62*, 1019–1040.

Wei, Q., and Adelstein, R. S. (2000). Conditional expression of a truncated fragment of nonmuscle myosin II-A alters cell shape but not cytokinesis in HeLa cells. Mol. Biol. Cell *11*, 3617–3627.

Xu, X., *et al*. (2005). ASF/SF2-regulated CaMKIIdelta alternative splicing temporally reprograms excitation-contraction coupling in cardiac muscle. Cell *120*, 59–72.